

## Flux variations of cosmic ray air showers detected by LHAASO-KM2A during thunderstorms

Xunxiu Zhou,\* Ci Yang, Xuejian Chen and Daihui Huang (on behalf of the LHAASO Collaboration)

*School of Physical Science and Technology, Southwest Jiaotong University, Chengdu 610031, China*

*E-mail: [zhouxx@swjtu.edu.cn](mailto:zhouxx@swjtu.edu.cn), [yangci@my.swjtu.edu.cn](mailto:yangci@my.swjtu.edu.cn)*

**Abstract:** The Large High Altitude Air Shower Observatory (LHAASO) has three sub-arrays, KM2A, WCDA and WFCTA, located at 4410 m above sea level in Sichuan Province, China. The high-altitude location and the frequent occurrence of thunderstorms make LHAASO suitable to study the effects of atmospheric electric fields (AEFs) on cosmic ray air showers. By analyzing the data of KM2A, the flux variations of cosmic ray air showers during thunderstorms are studied. The total number of shower events that meet the KM2A trigger conditions increases significantly during thunderstorms, with the maximum value exceeding 20%. The variations of trigger rates are found to be strongly dependent on the primary zenith angle. To understand the shower rate changes, the flux variations of ground-level secondary particles are analyzed. We find the average number of particles per shower event increases significantly in strong AEFs. Due to the acceleration by AEFs, the number of secondary particles with energy above the detector threshold increases, and then more shower events satisfy the trigger conditions, resulting in the shower rate increases. At the same time, the secondary particles carrying positive and negative charges will be deflected in opposite direction in AEFs, and this effect increases with the zenith angle. As a result, the flux variations of shower events detected by KM2A are correlated with the primary direction.

**Keywords:** LHAASO-KM2A, Cosmic rays, Thunderstorms

38th International Cosmic Ray Conference (ICRC2023)  
26 July - 3 August, 2023  
Nagoya, Japan



---

\*Speaker

## 1. Introduction

Thunderstorms, accompanied by intense lightning flashes and heavy rain [1], are common convective weather. During thunderstorms, the AEFs will change dramatically in contrast to fair weather [2]. The strength could be up to 1000 V/cm or even higher [3, 4], and the polarity can change multiple times [5]. Due to acceleration or deceleration by the strong electric fields in thunderclouds, the number and energies of secondary particles in extensive air showers (EAS) could be modified [6, 7, 8]. Because the charged particles are deflected, the space-time distribution at the ground-level will also be changed [9]. As a result, for ground-based experiments, the flux of shower events that meet the trigger conditions will change [10, 11, 12].

During a thunderstorm, due to the influence of lightning flashes and rain[13], the noise trigger recorded by the detector will increase. Considering the complex correlations between cosmic ray variations and thunderstorms, further data analyses and more simulation studies are needed. LHAASO is located at high altitude with frequent thunderstorms [14]. This unique geographical location is advantageous for observing the AEF effects on cosmic ray air showers. In this work, we study the flux variations of shower events and ground-level particles detected by LHAASO-KM2A during thunderstorms.

## 2. The LHAASO-KM2A Experiment

LHAASO, a new generation multi-purpose experiment[15], is sitting at 4410 m a.s.l. on the Haizi mountain, Sichuan province, China. As the main part of LHAASO, KM2A consists of 5216 electromagnetic particle detectors (EDs) and 1188 muon detectors (MDs), which are constructed and merged into the data acquisition system (DAQ) in stages. On 1 December 2020, the 3/4 KM2A array (including 3978 EDs and 917 MDs) started running. And the whole array began operating stably on 20 July 2021.

To study the cosmic ray variations during thunderstorms, a ground-based electric field monitor (EFM-1) was installed on the roof of the WCDA-2 building in September 2019. It is designed to measure the AEF with a saturation value of  $\pm 270$  V/cm [16]. Another electric field monitor (EFM-2) was mounted flush with the surface of the ground in October 2021, and the dynamic range of AEF measurement has been extended to  $\pm 1000$  V/cm. In this work, we define a positive AEF as the direction pointing towards the ground.

## 3. Observation Results

To know more about the correlation between the near-earth electric fields and cosmic ray variations detected by LHAASO-KM2A, three typical thunderstorm events that occurred on 10 June 2021 (Thunderstorm 20210610), 7 June 2022 (Thunderstorm 20220607), and 12 June 2022 (Thunderstorm 20220612) are analyzed in this work.

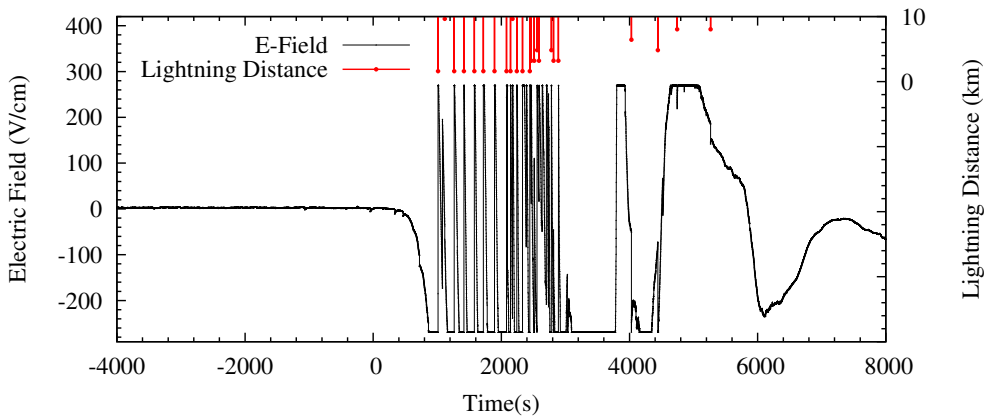
### 3.1 Shower rate variations during thunderstorms

In the shower mode, the KM2A detector is triggered when at least 20 EDs fired within a time window of 400 ns. The information on the arrival time and location of the signals from all the

EDs and MDs is recorded. The shower's arrival direction and core position are reconstructed by analyzing the ED signals[17]. And shower data are used for gamma ray astronomy and cosmic ray studies. During thunderstorms, due to the acceleration/deceleration and deflection by AEFs, the secondary particles in EAS are strongly affected. As a result, the number of shower events that meet the KM2A trigger conditions will also change. The observation results are shown as follows.

### 3.1.1 The electric field dependence of the shower rate variation

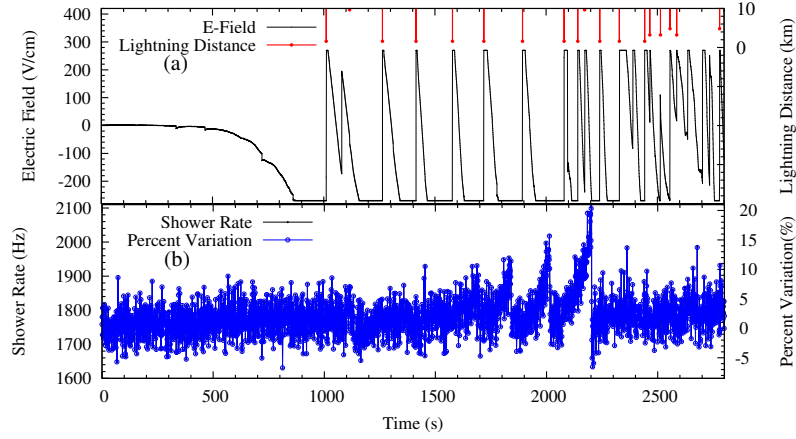
As a complex and notable episode, Thunderstorm 20210610 lasted for more than two hours, from 10:15:36 to 12:42:48 (UT) on 10 June 2021, with a long time of field strength in saturation and the polarity of the electric field changing frequently. The AEF variations are presented in Fig. 1. There were many lightning strikes estimated by EFM-1. For ground-based experiments, due to the heavy atmospheric attenuation[18], the cosmic ray variations are small when the thundercloud is far from the detector. Thus, we only consider the effects of near-earth AEF and nearby lightning strikes on the cosmic rays measured by KM2A in this paper. The 24 lightning strikes within 10 km are also shown in Fig. 1.



**Fig. 1.** Variations in the near-earth AEF and distance to the lightning strike (<10 km) recorded by EFM-1 during Thunderstorm 20210610. Time zero of the x-axis is 10:10:00 UT

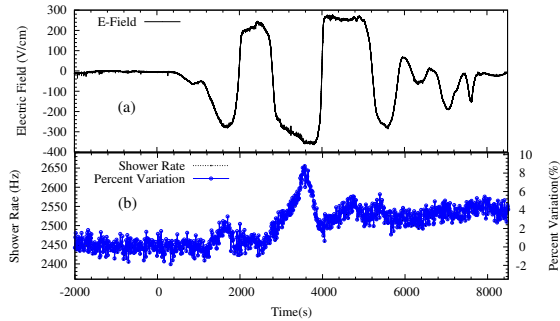
To study the electric field effects on cosmic rays, the operational status of detectors was carefully checked. Due to the strong lightning strikes, some detectors were powered off. We found that approximately 8% of the detectors were not working properly after 10:57:06.

Fig. 2 shows the distributions of the AEF, lightning distance, and shower rate detected by KM2A. We can see that the AEF intensity exceeded the measuring range of the EFM-1 several times and there were 11 nearby lightning strikes (with distances less than 1.6 km) from 720 to 2826 s. With respect to the shower rate measured in a period of 2000 s before the thunderstorm (defined as fair weather), the percent variations of shower rate are calculated. From Fig. 2 (b), it can be seen that the shower rate significantly increases in thunderstorm fields, with the maximum value exceeding 20%. More details can be found in our previous paper [11].



**Fig. 2.** Variations in AEF, distance to lightning strike(a), and shower rate (b) per second during Thunderstorm 20210610.

Thunderstorm 20220607, another typical one, lasted for about 2 hours. The distributions of the AEF recorded by EFM-2 are shown in Fig. 3 (a). The maximum value of the field is larger than 360 V/cm. As shown in Fig. 3, the time zero of the  $x$ -axis is set at 17:50:00 UT on 7 June 2022. The shower rate increases significantly, and the maximum value is up to 8% when the negative AEF reached -360 V/cm at 3570 s. In a positive field, the shower rate increases with smaller amplitude. For Thunderstorm 20220612, as shown in Fig. 4, the maximum strength of the electric field is up to 870 V/cm, there were multiple lightning strikes estimated by EFM-2 within 10 km. And time zero of the  $x$ -axis is set at 10:40:00 UT on 12 June 2022. It can be seen that the shower rate also increases in a negative electric field, with the maximum enhancement by up to 15%.



**Fig. 3.** Variations in AEF, distance to lightning strike(a) and shower rate (b) per second during Thunderstorm 20220607.

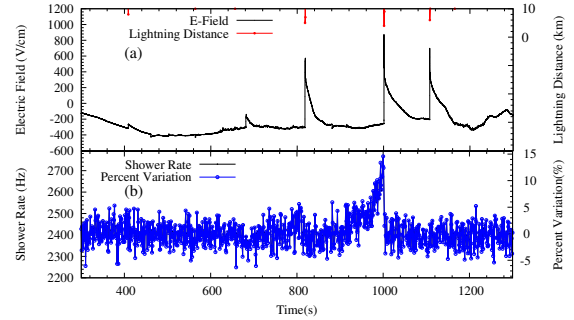


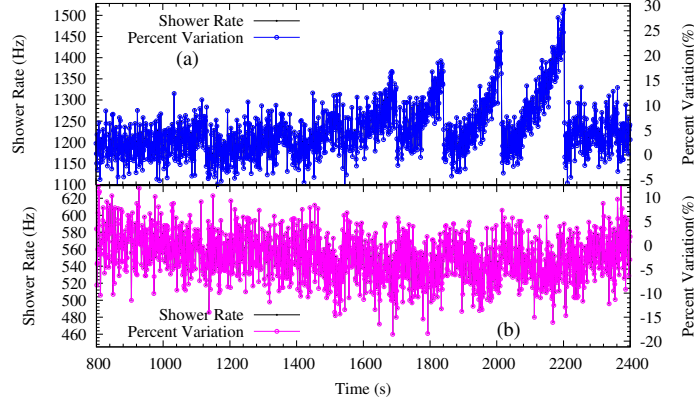
**Fig. 4.** Variations in AEF(a) and shower rate (b) per second during Thunderstorm 20220612.

From above, we can see the flux of shower events triggered by LHAASO-KM2A increases significantly during thunderstorms, and the amplitude is related to the strength and polarity of the AEF.

### 3.1.2 The zenith angle dependence of the shower rate variation

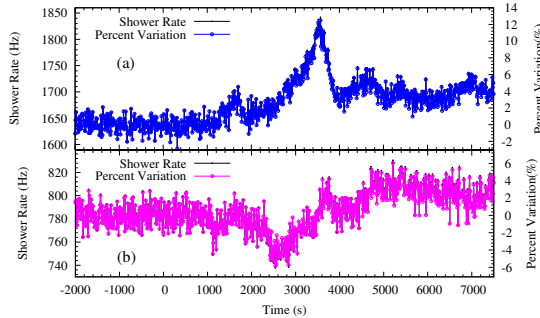
From references[18, 19], we can see that the AEFs have different effects on cosmic rays with different zenith angles ( $\theta$ ). By analyzing the reconstructed events in KM2A with the zenith angles less than  $60^\circ$ , the variations of shower rate during Thunderstorm 20210610 are shown in

Fig. 5. It can be seen that the trigger rate shows structural increases in the lower zenith angle ranges ( $0^\circ < \theta \leq 30^\circ$ ), with the maximum exceeding 29%. Whereas, for higher zenith angle ranges ( $30^\circ < \theta \leq 60^\circ$ ), we can clearly see the opposite variations, with it decreases up to -18%.



**Fig. 5.** The shower rate variations per second in zenith angle ranges of  $0\text{-}30^\circ$ (a) and  $30\text{-}60^\circ$  (b) during Thunderstorm 20210610

Similarly, during Thunderstorm 20220607 and Thunderstorm 20220612, the shower event variations in different zenith angle ranges are also analyzed (as shown in Fig. 6 and Fig. 7, respectively). For zenith angle ranges  $0\text{-}30^\circ$ , the shower rates increase, and the amplitude reaches 12% during Thunderstorm 20220607 and 20% during Thunderstorm 20220612. However, for larger zenith angle ranges  $30\text{-}60^\circ$ , the decreasing phenomena are observed for the two thunderstorms, and the amplitudes are up to -6% and -15%, respectively.



**Fig. 6.** The shower rate variations per second in zenith angle ranges of  $0\text{-}30^\circ$  (a) and  $30\text{-}60^\circ$  (b) during Thunderstorm 20220607.

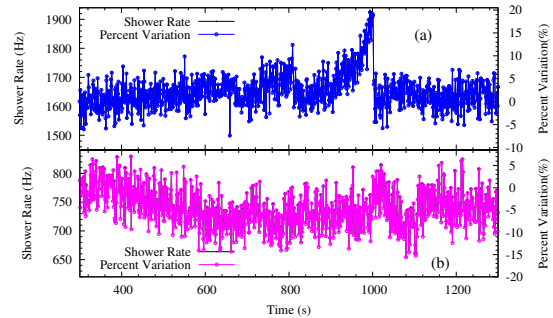


**Fig. 7.** The shower rate variations per second in zenith angle ranges of  $0\text{-}30^\circ$  (a) and  $30\text{-}60^\circ$  (b) during Thunderstorm 20220612.

### 3.2 The variations of secondary particles during thunderstorms

During thunderstorms, the flux of secondary particles with energy above the detector threshold is modified. At the same time, due to the sharply changing AEF, the detector noise will also increase. To understand the AEF effects on secondary cosmic rays, detailed studies on the variations of ground-level particles are necessary.

### 3.2.1 Intensity variations of secondary particles during thunderstorms

For each shower event, the trigger time is set at 0, and the DAQ records all hits within 5000 ns before or after the trigger time. According to the trigger logic, the data are divided into two parts. Most hits ( $N_{\text{off}}$ ) between -5000 and -1000 ns are noise, while the hits ( $N_{\text{on}}$ ) from -1000 to 5000 ns are mainly signals.

From  $N_{\text{on}}$  and  $N_{\text{off}}$ , the secondary particles ( $N_s$ ) from EAS can be calculated by the formula:

$$N_s = N_{\text{on}} - 1.5 \cdot N_{\text{off}}, \quad (1)$$

where  $1.5 = 6000/4000$  is the ratio between the widths of time windows. After considering the noise, the  $N_s$  during Thunderstorm 20210610 still shows a structural increase in strong negative fields, with a maximum value up to 20%, as shown in Fig. 8.

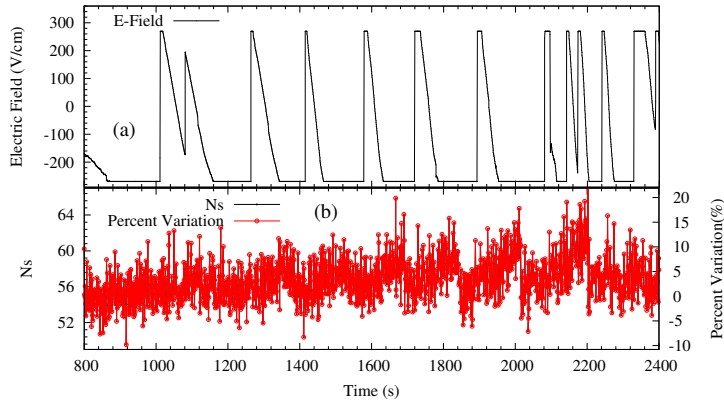


**Fig. 8.** Variations in AEFs (a) and  $N_s$  (b) per second during Thunderstorm 20210610.

### 3.2.2 Deflections of secondary particles during thunderstorms

Due to the transverse momentum of the secondary particles emerging from the collisions and scattering processes, the cascade spreads out laterally as well. The lateral spread of the particles is very large and can cover an area of up to several square kilometers [20]. The particle density drops rapidly with the increasing distance from shower core ( $r$ ). For ground-based experiments, the lateral distribution is important for reconstructing the shower's core location and arrival direction.

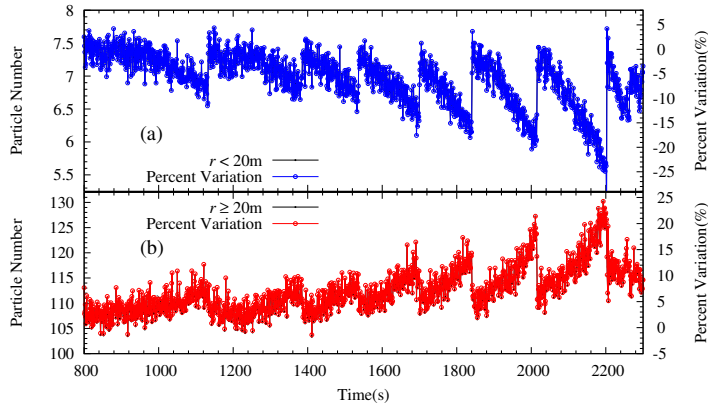


**Fig. 9.** Variations of secondary particles per second for  $r < 20$  m (a) and  $r \geq 20$  m (b) during Thunderstorm 20210610.

Fig. 9 shows the particle number (in one shower event) as a function of time in different core distance ranges during Thunderstorm 20210610. The flux decreases due to AEFs in the region of  $r < 20$  m, and the maximum decreasing value exceeds  $-25\%$ . For  $r \geq 20$  m, the flux increases and the maximum amplitude exceeds  $24\%$ .

The variations of the counting number as a function of the core distance are shown in Fig. 10. The particle number in fair weather is the mean value in 2000 s before the thunderstorm. For thunderstorm duration, the counting number is the average value in saturated negative fields. Near the shower core region, we can see the obvious decreasing phenomenon in fields. As the distance from the core increases beyond 60 m, however, the opposite situation occurs, the counting rate increases and the variation amplitude reaches the maximum of  $11\%$  at  $\sim 200$  m.

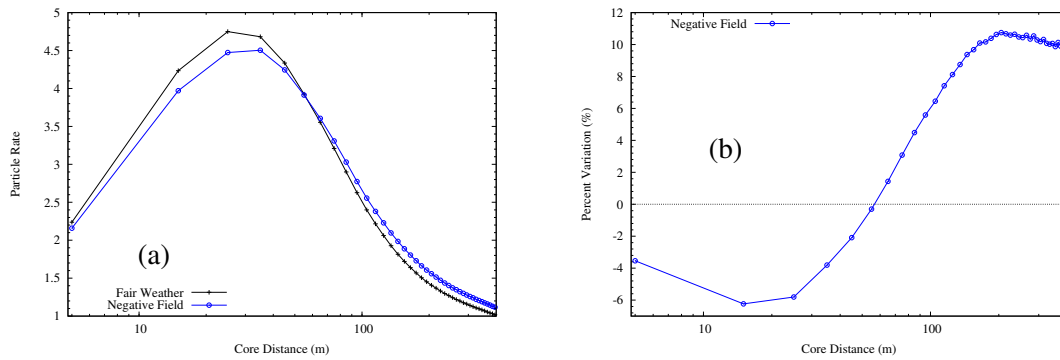


**Fig. 10.** The particle number distributions (a) and percent variations in saturated negative fields (b) as a function of core distance (10 m/bin).

Due to the deflection by the AEF, the lateral spread of the secondary particles is broadened during thunderstorms. In general, the AEF in thunderclouds is a vertical one, which has a more significant deflection effect on the inclined showers. As a result, the shower rate variations are related to the zenith angle.

#### 4. Summary

In this work, the cosmic ray variations detected by LHAASO-KM2A during thunderstorms are studied. Significant increase of the shower rates is observed by analyzing three different thunderstorms, with maximum amplitudes of  $20\%$ ,  $8\%$  and  $15\%$ . The variations are also dependent on the zenith angle. For smaller zenith angle ranges, the shower rate increases significantly, but decreasing situation occurs at larger zenith angle ranges. Meanwhile the flux increases of ground-level particles are observed, with the maximum enhancement of  $20\%$  (after considering the influence of noise).

Due to the acceleration/deceleration and deflection effects of the AEF on the charged particles from an EAS, our data can be understood. During thunderstorms, the number and positions of particle hits on the detector change, leading to the trigger rate changes. Considering a vertical AEF in thunderclouds, the deflection effects on the charged particles from inclined showers are larger. For a given detector, the shower rate variations are related to the zenith angle.

## Acknowledgments

This work is supported by the National Natural Science Foundation of China (NSFC) under the Grant No. U2031101, and the National Key R&D Program of China under the grant No.2018YFA0404201. The authors would like to express their sincere thanks to the members of the LHAASO collaboration.

## References

- [1] X. S. Qie et al., *Sci. China Earth Sci.* **64**, 10 (2021).
- [2] R. I. Huang et al., *Journal of Sichuan Normal University*, **45**(06), 784-789 (2022).
- [3] T. C. Marshall et al., *Geophys. Res. Lett.*, **32**, L03813 (2005).
- [4] A. Chilingarian et al., *Phys. Rev. D*, **103**, 043021 (2021).
- [5] J. F. Wang et al., *Acta. Phys. Sin.*, **61**, 159202 (2012).
- [6] K. Kudela et al., *J. Geophys. Res.*, **122**, 10700 (2017).
- [7] X. X. Zhou et al., *Astropart. Phys.*, **84**, 107 (2016).
- [8] R. R. Yan et al., *Chin. J. Astron. Astrophys.*, **44**(2), 146-159 (2020).
- [9] K. G. Axi et al., *Astrophys. Space Sci.*, **367**, 30 (2022).
- [10] S. Vernetto for EAS-TOP Collaboration, 27th ICRC, **10**, 4165 (2001).
- [11] F. Aharonian et al. (LHAASO Collaboration), *Chin. Phys. C*, **47**, 015001 (2023).
- [12] Axikegu et al. (ARGO-YBJ Collaboration), *Phys. Rev. D*, **106**, 022008 (2022).
- [13] A. Chilingarian et al., *Phys. Rev. D*, **98**, 082001 (2018).
- [14] Z. Cao et al., *Acta. Astronom. Sin.*, **43**, 457-478 (2019).
- [15] D. della Volpe. *Journal of Physics*, **2429**, 1 (2023).
- [16] [https://www.boltek.com/EFM-100C\\_Manual\\_121415.pdf](https://www.boltek.com/EFM-100C_Manual_121415.pdf), retrieved 12 June 2023
- [17] F. Aharonian et al. (LHAASO Collaboration), *Chin. Phys. C*, **45**, 025002 (2021).
- [18] X. X. Zhou et al., *Chin. J. Space Sci.*, **36**(1), 49-55 (2016) (in Chinese).
- [19] S. Buitink et al., *Astropart. Phys.*, **33**(1), 1-12 (2010).
- [20] K. F. Grieder Peter, Springer-Verlag Berlin Heidelberg, **1**, 3 (2010).

**Full Authors List: LHAASO Collaboration**

Zhen Cao<sup>1,2,3</sup>, F. Aharonian<sup>4,5</sup>, Q. An<sup>6,7</sup>, Axikegu<sup>8</sup>, Y.X. Bai<sup>1,3</sup>, Y.W. Bao<sup>9</sup>, D. Bastieri<sup>10</sup>, X.J. Bi<sup>1,2,3</sup>, Y.J. Bi<sup>1,3</sup>, J.T. Cai<sup>10</sup>, Q. Cao<sup>11</sup>, W.Y. Cao<sup>7</sup>, Zhe Cao<sup>6,7</sup>, J. Chang<sup>12</sup>, J.F. Chang<sup>1,3,6</sup>, A.M. Chen<sup>13</sup>, E.S. Chen<sup>1,2,3</sup>, Liang Chen<sup>14</sup>, Lin Chen<sup>8</sup>, Long Chen<sup>8</sup>, M.J. Chen<sup>1,3</sup>, M.L. Chen<sup>1,3,6</sup>, Q.H. Chen<sup>8</sup>, S.H. Chen<sup>1,2,3</sup>, S.Z. Chen<sup>1,3</sup>, T.L. Chen<sup>15</sup>, Y. Chen<sup>9</sup>, N. Cheng<sup>1,3</sup>, Y.D. Cheng<sup>1,3</sup>, M.Y. Cui<sup>12</sup>, S.W. Cui<sup>11</sup>, X.H. Cui<sup>16</sup>, Y.D. Cui<sup>17</sup>, B.Z. Dai<sup>18</sup>, H.L. Dai<sup>1,3,6</sup>, Z.G. Dai<sup>7</sup>, Danzengluobu<sup>15</sup>, D. della Volpe<sup>19</sup>, X.Q. Dong<sup>1,2,3</sup>, K.K. Duan<sup>12</sup>, J.H. Fan<sup>10</sup>, Y.Z. Fan<sup>12</sup>, J. Fang<sup>18</sup>, K. Fang<sup>1,3</sup>, C.F. Feng<sup>20</sup>, L. Feng<sup>12</sup>, S.H. Feng<sup>1,3</sup>, X.T. Feng<sup>20</sup>, Y.L. Feng<sup>15</sup>, S. Gabici<sup>21</sup>, B. Gao<sup>1,3</sup>, C.D. Gao<sup>20</sup>, L.Q. Gao<sup>1,2,3</sup>, Q. Gao<sup>15</sup>, W. Gao<sup>1,3</sup>, W.K. Gao<sup>1,2,3</sup>, M.M. Ge<sup>18</sup>, L.S. Geng<sup>1,3</sup>, G. Giacinti<sup>13</sup>, G.H. Gong<sup>22</sup>, Q.B. Gou<sup>1,3</sup>, M.H. Gu<sup>1,3,6</sup>, F.L. Guo<sup>14</sup>, X.L. Guo<sup>8</sup>, Y.Q. Guo<sup>1,3</sup>, Y.Y. Guo<sup>12</sup>, Y.A. Han<sup>23</sup>, H.H. He<sup>1,2,3</sup>, H.N. He<sup>12</sup>, J.Y. He<sup>12</sup>, X.B. He<sup>17</sup>, Y. He<sup>8</sup>, M. Heller<sup>19</sup>, Y.K. Hor<sup>17</sup>, B.W. Hou<sup>1,2,3</sup>, C. Hou<sup>1,3</sup>, X. Hou<sup>24</sup>, H.B. Hu<sup>1,2,3</sup>, Q. Hu<sup>7,12</sup>, S.C. Hu<sup>1,2,3</sup>, D.H. Huang<sup>8</sup>, T.Q. Huang<sup>1,3</sup>, W.J. Huang<sup>17</sup>, X.T. Huang<sup>20</sup>, X.Y. Huang<sup>12</sup>, Y. Huang<sup>1,2,3</sup>, Z.C. Huang<sup>8</sup>, X.L. Ji<sup>1,3,6</sup>, H.Y. Jia<sup>8</sup>, K. Jia<sup>20</sup>, K. Jiang<sup>6,7</sup>, X.W. Jiang<sup>1,3</sup>, Z.J. Jiang<sup>18</sup>, M. Jin<sup>8</sup>, M.M. Kang<sup>25</sup>, T. Ke<sup>1,3</sup>, D. Kuleshov<sup>26</sup>, K. Kurinov<sup>26</sup>, B.B. Li<sup>11</sup>, Cheng Li<sup>6,7</sup>, Cong Li<sup>1,3</sup>, D. Li<sup>1,2,3</sup>, F. Li<sup>1,3,6</sup>, H.B. Li<sup>1,3</sup>, H.C. Li<sup>1,3</sup>, H.Y. Li<sup>7,12</sup>, J. Li<sup>7,12</sup>, Jian Li<sup>7</sup>, Jie Li<sup>1,3,6</sup>, K. Li<sup>1,3</sup>, W.L. Li<sup>20</sup>, W.L. Li<sup>13</sup>, X.R. Li<sup>1,3</sup>, Xin Li<sup>6,7</sup>, Y.Z. Li<sup>1,2,3</sup>, Zhe Li<sup>1,3</sup>, Zhuo Li<sup>27</sup>, E.W. Liang<sup>28</sup>, Y.F. Liang<sup>28</sup>, S.J. Lin<sup>17</sup>, B. Liu<sup>7</sup>, C. Liu<sup>1,3</sup>, D. Liu<sup>20</sup>, H. Liu<sup>8</sup>, H.D. Liu<sup>23</sup>, J. Liu<sup>1,3</sup>, J.L. Liu<sup>1,3</sup>, J.Y. Liu<sup>1,3</sup>, M.Y. Liu<sup>15</sup>, R.Y. Liu<sup>9</sup>, S.M. Liu<sup>8</sup>, W. Liu<sup>1,3</sup>, Y. Liu<sup>10</sup>, Y.N. Liu<sup>22</sup>, R. Lu<sup>18</sup>, Q. Luo<sup>17</sup>, H.K. Lv<sup>1,3</sup>, B.Q. Ma<sup>27</sup>, L.L. Ma<sup>1,3</sup>, X.H. Ma<sup>1,3</sup>, J.R. Mao<sup>24</sup>, Z. Min<sup>1,3</sup>, W. Mitthumsiri<sup>29</sup>, H.J. Mu<sup>23</sup>, Y.C. Nan<sup>1,3</sup>, A. Neronov<sup>21</sup>, Z.W. Ou<sup>17</sup>, B.Y. Pang<sup>8</sup>, P. Pattarakijwanich<sup>29</sup>, Z.Y. Pei<sup>10</sup>, M.Y. Qi<sup>1,3</sup>, Y.Q. Qi<sup>11</sup>, B.Q. Qiao<sup>1,3</sup>, J.J. Qin<sup>7</sup>, D. Ruffolo<sup>29</sup>, A. Sáiz<sup>29</sup>, D. Semikoz<sup>21</sup>, C.Y. Shao<sup>17</sup>, L. Shao<sup>11</sup>, O. Shchegolev<sup>26,30</sup>, X.D. Sheng<sup>1,3</sup>, F.W. Shu<sup>31</sup>, H.C. Song<sup>27</sup>, Yu.V. Stenkin<sup>26,30</sup>, V. Stepanov<sup>26</sup>, Y. Su<sup>12</sup>, Q.N. Sun<sup>8</sup>, X.N. Sun<sup>28</sup>, Z.B. Sun<sup>32</sup>, P.H.T. Tam<sup>17</sup>, Q.W. Tang<sup>31</sup>, Z.B. Tang<sup>6,7</sup>, W.W. Tian<sup>2,16</sup>, C. Wang<sup>32</sup>, C.B. Wang<sup>8</sup>, G.W. Wang<sup>7</sup>, H.G. Wang<sup>10</sup>, H.H. Wang<sup>17</sup>, J.C. Wang<sup>24</sup>, K. Wang<sup>9</sup>, L.P. Wang<sup>20</sup>, L.Y. Wang<sup>1,3</sup>, P.H. Wang<sup>8</sup>, R. Wang<sup>20</sup>, W. Wang<sup>17</sup>, X.G. Wang<sup>28</sup>, X.Y. Wang<sup>9</sup>, Y. Wang<sup>8</sup>, Y.D. Wang<sup>1,3</sup>, Y.J. Wang<sup>1,3</sup>, Z.H. Wang<sup>25</sup>, Z.X. Wang<sup>18</sup>, Zhen Wang<sup>13</sup>, Zheng Wang<sup>1,3,6</sup>, D.M. Wei<sup>12</sup>, J.J. Wei<sup>12</sup>, Y.J. Wei<sup>1,2,3</sup>, T. Wen<sup>18</sup>, C.Y. Wu<sup>1,3</sup>, H.R. Wu<sup>1,3</sup>, S. Wu<sup>1,3</sup>, X.F. Wu<sup>12</sup>, Y.S. Wu<sup>7</sup>, S.Q. Xi<sup>1,3</sup>, J. Xia<sup>7,12</sup>, J.J. Xia<sup>8</sup>, G.M. Xiang<sup>2,14</sup>, D.X. Xiao<sup>11</sup>, G. Xiao<sup>1,3</sup>, G.G. Xin<sup>1,3</sup>, Y.L. Xin<sup>8</sup>, Y. Xing<sup>14</sup>, Z. Xiong<sup>1,2,3</sup>, D.L. Xu<sup>13</sup>, R.F. Xu<sup>1,2,3</sup>, R.X. Xu<sup>27</sup>, W.L. Xu<sup>25</sup>, L. Xue<sup>20</sup>, D.H. Yan<sup>18</sup>, J.Z. Yan<sup>12</sup>, T. Yan<sup>1,3</sup>, C.W. Yang<sup>25</sup>, F. Yang<sup>11</sup>, F.F. Yang<sup>1,3,6</sup>, H.W. Yang<sup>17</sup>, J.Y. Yang<sup>17</sup>, L.L. Yang<sup>17</sup>, M.J. Yang<sup>1,3</sup>, R.Z. Yang<sup>7</sup>, S.B. Yang<sup>18</sup>, Y.H. Yao<sup>25</sup>, Z.G. Yao<sup>1,3</sup>, Y.M. Ye<sup>22</sup>, L.Q. Yin<sup>1,3</sup>, N. Yin<sup>20</sup>, X.H. You<sup>1,3</sup>, Z.Y. You<sup>1,3</sup>, Y.H. Yu<sup>7</sup>, Q. Yuan<sup>12</sup>, H. Yue<sup>1,2,3</sup>, H.D. Zeng<sup>12</sup>, T.X. Zeng<sup>1,3,6</sup>, W. Zeng<sup>18</sup>, M. Zha<sup>1,3</sup>, B.B. Zhang<sup>9</sup>, F. Zhang<sup>8</sup>, H.M. Zhang<sup>9</sup>, H.Y. Zhang<sup>1,3</sup>, J.L. Zhang<sup>16</sup>, L.X. Zhang<sup>10</sup>, Li Zhang<sup>18</sup>, P.F. Zhang<sup>18</sup>, P.P. Zhang<sup>7,12</sup>, R. Zhang<sup>7,12</sup>, S.B. Zhang<sup>2,16</sup>, S.R. Zhang<sup>11</sup>, S.S. Zhang<sup>1,3</sup>, X. Zhang<sup>9</sup>, X.P. Zhang<sup>1,3</sup>, Y.F. Zhang<sup>8</sup>, Yi Zhang<sup>1,12</sup>, Yong Zhang<sup>1,3</sup>, B. Zhao<sup>8</sup>, J. Zhao<sup>1,3</sup>, L. Zhao<sup>6,7</sup>, L.Z. Zhao<sup>11</sup>, S.P. Zhao<sup>12,20</sup>, F. Zheng<sup>32</sup>, B. Zhou<sup>1,3</sup>, H. Zhou<sup>13</sup>, J.N. Zhou<sup>14</sup>, M. Zhou<sup>31</sup>, P. Zhou<sup>9</sup>, R. Zhou<sup>25</sup>, X.X. Zhou<sup>8</sup>, C.G. Zhu<sup>20</sup>, F.R. Zhu<sup>8</sup>, H. Zhu<sup>16</sup>, K.J. Zhu<sup>1,2,3,6</sup>, X. Zuo<sup>1,3</sup>, (The LHAASO Collaboration)

<sup>1</sup> Key Laboratory of Particle Astrophysics & Experimental Physics Division & Computing Center, Institute of High Energy Physics, Chinese Academy of Sciences, 100049 Beijing, China

<sup>2</sup> University of Chinese Academy of Sciences, 100049 Beijing, China

<sup>3</sup> TIANFU Cosmic Ray Research Center, Chengdu, Sichuan, China

<sup>4</sup> Dublin Institute for Advanced Studies, 31 Fitzwilliam Place, 2 Dublin, Ireland

<sup>5</sup> Max-Planck-Institut für Kernphysik, P.O. Box 103980, 69029 Heidelberg, Germany

<sup>6</sup> State Key Laboratory of Particle Detection and Electronics, China

<sup>7</sup> University of Science and Technology of China, 230026 Hefei, Anhui, China

<sup>8</sup> School of Physical Science and Technology & School of Information Science and Technology, Southwest Jiaotong University, 610031 Chengdu, Sichuan, China

<sup>9</sup> School of Astronomy and Space Science, Nanjing University, 210023 Nanjing, Jiangsu, China

<sup>10</sup> Center for Astrophysics, Guangzhou University, 510006 Guangzhou, Guangdong, China

<sup>11</sup> Hebei Normal University, 050024 Shijiazhuang, Hebei, China

<sup>12</sup> Key Laboratory of Dark Matter and Space Astronomy & Key Laboratory of Radio Astronomy, Purple Mountain Observatory, Chinese Academy of Sciences, 210023 Nanjing, Jiangsu, China

<sup>13</sup> Tsung-Dao Lee Institute & School of Physics and Astronomy, Shanghai Jiao Tong University, 200240 Shanghai, China

<sup>14</sup> Key Laboratory for Research in Galaxies and Cosmology, Shanghai Astronomical Observatory, Chinese Academy of Sciences, 200030 Shanghai, China

- <sup>15</sup> Key Laboratory of Cosmic Rays (Tibet University), Ministry of Education, 850000 Lhasa, Tibet, China
- <sup>16</sup> National Astronomical Observatories, Chinese Academy of Sciences, 100101 Beijing, China
- <sup>17</sup> School of Physics and Astronomy (Zhuhai) & School of Physics (Guangzhou) & Sino-French Institute of Nuclear Engineering and Technology (Zhuhai), Sun Yat-sen University, 519000 Zhuhai & 510275 Guangzhou, Guangdong, China
- <sup>18</sup> School of Physics and Astronomy, Yunnan University, 650091 Kunming, Yunnan, China
- <sup>19</sup> Département de Physique Nucléaire et Corpusculaire, Faculté de Sciences, Université de Genève, 24 Quai Ernest Ansermet, 1211 Geneva, Switzerland
- <sup>20</sup> Institute of Frontier and Interdisciplinary Science, Shandong University, 266237 Qingdao, Shandong, China
- <sup>21</sup> APC, Université Paris Cité, CNRS/IN2P3, CEA/IRFU, Observatoire de Paris, 119 75205 Paris, France
- <sup>22</sup> Department of Engineering Physics, Tsinghua University, 100084 Beijing, China
- <sup>23</sup> School of Physics and Microelectronics, Zhengzhou University, 450001 Zhengzhou, Henan, China
- <sup>24</sup> Yunnan Observatories, Chinese Academy of Sciences, 650216 Kunming, Yunnan, China
- <sup>25</sup> College of Physics, Sichuan University, 610065 Chengdu, Sichuan, China
- <sup>26</sup> Institute for Nuclear Research of Russian Academy of Sciences, 117312 Moscow, Russia
- <sup>27</sup> School of Physics, Peking University, 100871 Beijing, China
- <sup>28</sup> School of Physical Science and Technology, Guangxi University, 530004 Nanning, Guangxi, China
- <sup>29</sup> Department of Physics, Faculty of Science, Mahidol University, Bangkok 10400, Thailand
- <sup>30</sup> Moscow Institute of Physics and Technology, 141700 Moscow, Russia
- <sup>31</sup> Center for Relativistic Astrophysics and High Energy Physics, School of Physics and Materials Science & Institute of Space Science and Technology, Nanchang University, 330031 Nanchang, Jiangxi, China
- <sup>32</sup> National Space Science Center, Chinese Academy of Sciences, 100190 Beijing, China